Earth and Planetary Science Letters 420 (2015) 102–115

Contents lists available at ScienceDirect

Earth and Planetary Science Letters

www.elsevier.com/locate/epsl

Implications of reduced turbidity current and landslide activity for the Initial Eocene Thermal Maximum – evidence from two distal, deep-water sites

Michael A. Clare *, Peter J. Talling, James E. Hunt

National Oceanography Centre, Southampton, European Way, Southampton, SO14 3ZH, UK

ARTICLE INFO

Article history:
Received 8 May 2014
Received in revised form 8 March 2015
Accepted 9 March 2015
Available online 3 April 2015
Editor: J. Lynch-Stieglitz

Keywords:
IETM
PETM
submarine landslide
gas hydrate
geohazard
global warming

ABSTRACT

Previous studies propose that submarine landslides and turbidity currents may become more likely due to future rapid global warming. Determining whether global warming increases likelihood assists in assessment of landslide-triggered tsunami hazards and risk to seafloor structures. Other studies propose that landslides helped to trigger past rapid climate change due to sudden release of gas hydrates. Two deep-water turbidite records show prolonged hiatuses in turbidity current activity during the Initial Eocene Thermal Maximum (IETM) at ~55 Ma. The IETM represents a possible proxy for future anthropogenically-induced climate change. It is likely that our records mainly represent large and fast moving disintegrative submarine landslides. Statistical analysis of long term (>2.3 Myr) records shows that turbidity current frequency significantly decreased after the IETM. Our results indicate that rapid climate change does not necessarily cause increased turbidity current activity, and do not provide evidence for landslides as a primary trigger for the IETM.

1. Introduction

A period of unusually rapid global warming occurred at ~55 Ma (McInerney and Wing, 2011), termed the Initial Eocene Thermal Maximum (IETM). This hyperthermal represents the warmest period on Earth during the Cenozoic (Schmitz et al., 2001), featuring, at its peak, a dramatic 6–8 °C warming of global deep waters over a period of approximately 10 kyr (Kennett and Stott, 1991). The IETM is marked globally by a negative carbon isotopic ratio ($\delta^{13}C$) excursion, which has been linked to methane emissions due to dissociation of gas hydrate in marine sediment. Other causal mechanisms have been invoked (Dunkley-Jones et al., 2010), but emissions of methane from marine hydrates are one of the most widely held explanations for IETM (Dickens et al., 1995; Katz et al., 1999, 2001). The IETM has been used as a proxy for present-day anthropogenically-induced global warming (Agnini at al., 2007; Dunkley-Jones et al., 2010).

Understanding changes in the frequency of landslides and turbidity currents in response to the IETM may help predict future changes in landslide and turbidity current frequency as climate warms. It has been proposed that rapid global warming will lead to significant increases in landslide and turbidity current frequency, due to gas hydrate dissociation in response to elevated ocean temperatures (Maslin et al., 1998; Nisbet and Piper, 1998; Owen et al., 2007; Lee, 2009; Maslin et al., 2010). Dissociation of gas hydrate can weaken slopes and increase the probability of slope failure (Grozic, 2010).

In addition to climate change causing variations in landslide or turbidity current frequency, it has been proposed that submarine landslides play a role in driving rapid climate change (Kennett et al., 2003; Maslin et al., 2004; Bock et al., 2012). These studies suggest that dissociation of gas hydrate within, or below, the failed slide material, may lead to significant emissions of methane (Katz et al., 1999; Hornbach et al., 2007; Maslin et al., 2010). It was proposed that release of methane (a strong greenhouse gas) from gas hydrate within marine sediment, due to landslides or other processes, was the major control on atmospheric methane abundance (Kennett et al., 2003). The validity of this "clathrate gun hypothesis" is contentious. Methane emissions from wetlands may exceed those from gas hydrates hosted in marine sediments, as suggested by isotopic analysis of methane within ice core records (Sowers, 2006). Here we consider whether our two study locations provide evidence that landslides may have helped to drive climate change through methane emissions. This has not previously been investigated using continuous turbidite records across well dated climatic excursions.

* Corresponding author. Tel.: +44 (0) 1491 820 869.
E-mail address: mac1y11@soton.ac.uk (M.A. Clare).

http://dx.doi.org/10.1016/j.epsl.2015.03.022

1.1. Turbidites as a record of disintegrative landslides

It is logistically difficult to accurately date a sufficient number of landslides (>100) around a basin margin for robust statistical analysis of recurrence intervals during the IETM. However, we have records of turbidity current frequency across the IETM, which contain distal landslide deposits. The large number (N = 285 to 421) of turbidites in our records enables statistical analysis of recurrence intervals. Turbidity currents can be triggered by a range of processes other than submarine landslides, however, such as storm waves and hyperpycnal river flood discharge (Normark and Piper, 1991; Piper and Normark, 2009; Talling et al., 2013). It is therefore important to assess the level of certainty that these turbidites are landslide triggered. Turbidity currents with suspended sediment volumes far in excess of the largest river floods are likely to be triggered by submarine landslides (Talling et al., 2007, 2014; Talling, 2014), although other triggers may cause flows that pick up sediment en-route. Individual turbidite beds cannot be mapped over large areas to determine volumes for either of our study areas. Thus, it cannot be shown unequivocally that our turbidites are landslide triggered. It is probable that some landslides occurred, but failed to disintegrate to form long run-out turbidity currents that reached our study areas. Therefore not all landslides are likely to be recorded in the datasets.

However, both datasets are inferred to come from distal basin plain depositional sequences, featuring minimal erosion (Weaver and Thomson, 1993; Whitmarsh et al., 1998; Schmitz et al., 2001). It is thought that landslides trigger many of the turbidites seen in other basin plain sequences, where volumes can be constrained (Elmore et al., 1979; Pilkey, 1988; Talling et al., 2007, 2012; Hunt et al., 2013; Clare et al., 2014) or cables have been damaged by flows (Piper and Savoye, 1993; Piper et al., 1999). It is thus reasonable to infer that a predominant fraction of turbidites within our basin plain sequences were triggered by landslides.

1.2. Geohazards and global sediment flux

Due to their potential volume and speed, submarine landslides can generate destructive tsunamis that cause fatalities, or damage expensive seafloor structures (Tappin et al., 2001; Bondevik et al., 2005). The morphology and extent of a landslide will affect its hazard potential. Deep-seated, fast moving landslides may be more prone to tsunami-genesis and release of gas hydrate, whereas more widespread, thinner failures triggered by seismic shaking may have a reduced influence. Regardless of initial mechanics, if a disintegrative landslide triggers a turbidity current, it may pose a hazard to pipelines and seafloor cable networks (Piper et al., 1999; Bruschi et al., 2006; Carter et al., 2012) that carry over 95% of transoceanic data traffic including the internet and financial services (Carter et al., 2009). Turbidity currents that result from disintegration of submarine landslides, as well as from other triggers, may reach speeds of up to 19 m/s (Piper et al., 1999). Understanding the frequency of submarine landslides and turbidity currents, regardless of trigger, is therefore important for geohazard assessments.

An individual landslide may comprise up to thousands of cubic kilometres of sediment, two orders of magnitude greater than the largest terrestrial landslides (Hühnerbach and Masson, 2004; Haflidason et al., 2005; Korup et al., 2007; Masson et al., 2010). Turbidity currents have also been shown to transport hundreds of cubic kilometres of sediment for several hundreds of kilometres (Talling et al., 2012). Submarine landslides and turbidity currents are therefore major contributors to global sediment flux.

1.3. Previous work

Of the previous studies that have attempted to quantify turbidity current recurrence frequency (e.g. Droxler and Schlager, 1985; Weaver et al., 1992; Beattie and Dade, 1996; Goldfinger et al., 2003; Romans et al., 2009; Atwater and Griggs, 2012), only a handful consider large numbers of events (N > 100) over long (>1 Myr) timescales (e.g. Weaver et al., 1986; Clare et al., 2014; Hunt et al., 2014). Submarine landslide frequency studies typically analyse fewer than ten events (e.g. Geist and Parsons, 2010). Exceptions exist with up to 68 dated events (e.g. Owen et al., 2007; Urlaub et al., 2013); however, these global databases only extend back in time to a maximum of 180 ka.

Despite this, many studies have drawn conclusions about the influence of variables such as sea level and global temperature variations on landslide recurrence rate (e.g. Owen et al., 2007; Brothers et al., 2013). Conversely, some studies have shown that non-random processes, such as sea level change, may not exert a dominant control on landslide (Geist and Parsons, 2010; Urlaub et al., 2013, 2014) and turbidite recurrence (Beattie and Dade, 1996; Hunt et al., 2013; Clare et al., 2014). To make more meaningful, quantitative inferences on triggering and conditioning factors, there is a need for statistically robust (N > 100) datasets of landslide ages to be acquired in a variety of settings.

2. Aims

Our first aim is to test whether rapid global ocean warming at the IETM (~ 55 Ma) coincides with an increase in turbidity current activity. This is to determine whether global warming may have promoted slope instability, or vice-versa through dissociation of gas hydrates. We analyse deep-water turbidite records (Fig. 1) from the Zumaia coastal outcrop in NE Spain (2.3 Myr) and from ODP borehole records on the Iberian Margin (5.5 Myr). Here we assume that these turbidity currents were mainly triggered by submarine landslides. The datasets contain sufficient bed quantities for statistical analysis (i.e. N > 100).

Secondly, we aim to determine if recurrence intervals of turbidity currents were significantly different prior to, and after, the IETM interval over a window of ~1 Myr. This is to assess if the IETM exerted a longer-term influence on turbidity current activity. Here we make no assumption on the nature of turbidity current trigger.

Thirdly, we aim to determine whether our results are consistent with previously published deep-water records across the IETM. We discuss the implications of our work for predicting future submarine landslide and turbidity current activity, and whether landslides may contribute to rapid climate change through gas hydrate dissociation and methane emissions.

3. Study areas

The datasets selected for this study satisfy four main criteria. Firstly, they represent a continuous sedimentary record including the IETM. Second, they feature sufficient (N > 100) turbidites for statistical analysis. Third, hemipelagic mud can be distinguished clearly from turbidite mud. This allows the cumulative thickness of hemipelagic mud to be measured, and used as a proxy for time between dated horizons in the stratigraphy. This method (Clare et al., 2014) allows turbidite recurrence times to be estimated. Fourth, the sections have good age dating.

The first site is a coastal exposure at Itzurun Beach, Zumaia in NE Spain (Fig. 1B). This is one of the most expanded and continuous sections through the IETM worldwide (Canudo and Molina, 1992; Canudo et al., 1995; Schmitz et al., 2001). A robust age and

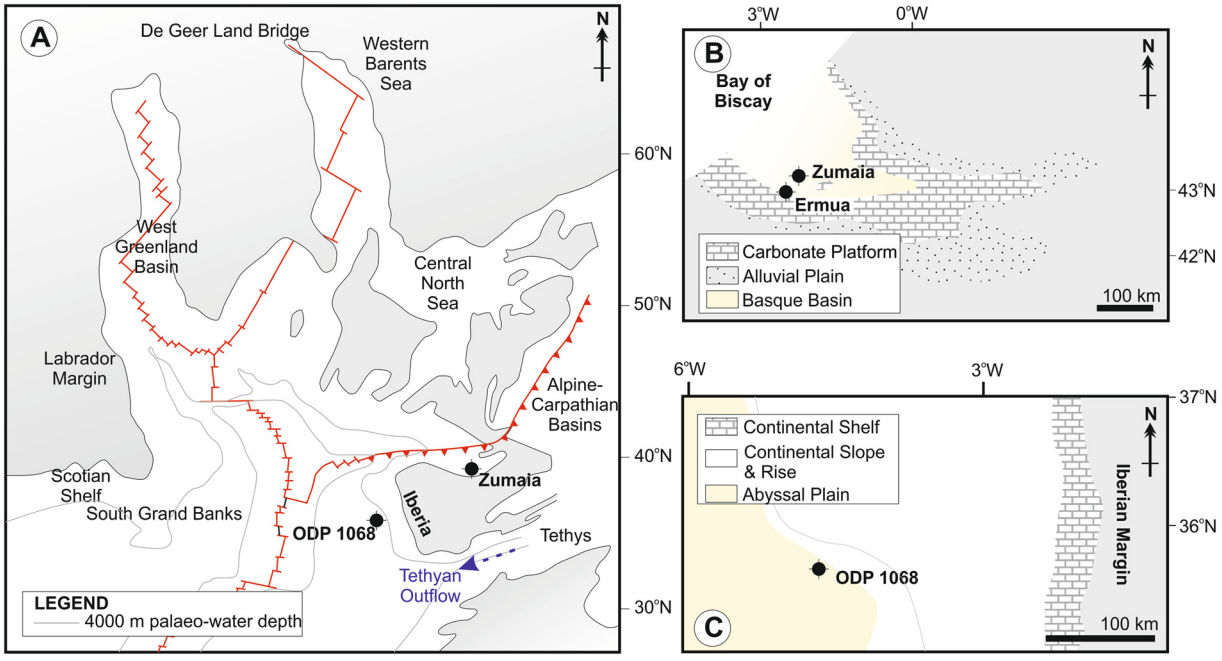

Fig. 1. Palaeogeographic reconstructions at the end-Palaeocene to show: (A) Relative location of sites (modified from Kaminski et al., 1989); (B) Zumaia and surrounding region (modified from Schmitz et al., 2001); (C) ODP Site 1068 (modified from Whitmarsh et al., 1998).

climate framework was developed from palaeoclimatic, palaeontologic, palaeoecologic and chronostratigraphic studies specifically for the Palaeocene and Eocene interval. During the IETM, Zumaia was part of a deep-water (>1000 m) marine basin (Winkler and Gawenda, 1999) flanked by mixed carbonate-terrigenous shelf systems (Fig. 1B), as verified by thinly interbedded, hemipelagic and distal calciclastic–siliciclastic turbidite deposits. The interval selected (54.0 to 56.3 Ma) at Zumaia avoids a faulted interval where stratigraphic repetition or omission may occur and terminates prior to a transition to a submarine fan setting, in which erosional bed amalgamation is common (Cummings and Hodgson, 2011). A coarse resolution study of turbidite frequency has previously been performed at Zumaia (Winkler and Gawenda, 1999; Gawenda and Winkler, 2000); however, it did not specifically focus on the IETM, nor were individual recurrence intervals calculated.

The second record comes from Ocean Drilling Program (ODP) Site 1068 located on the western flank of a N–S trending basement high near the southern edge of the Iberian Abyssal Plain (Fig. 1C; Whitmarsh et al., 1998). The setting during the IETM was that of a distal continental rise-abyssal plain transition dominated by hemipelagic muds with thin, interbedded turbidites (Whitmarsh et al., 1998). The studied interval of core extends from 51.0–56.5 Ma.

3.1. Regional tectonic setting

While the Palaeocene to early Eocene was relatively tectonically quiet at our study sites (Vergés et al., 1995; Rosenbaum et al., 2002), there is evidence of regional variation (see supplementary information). The most pronounced intervals of deformation postdate our study intervals, including mid to late Eocene (Masson et al., 1994) and Miocene compression (Pinheiro et al., 1996).

Africa and Europe began to converge at ~83 Ma, with movement of Iberia virtually ceasing from 67–55 Ma (Rosenbaum et al., 2002; Tugend et al., 2015). This period of quiescence crosses the IETM and the start of our study intervals.

Convergence resumed in Europe, when Iberia shifted to northwestward transpression at ~55 Ma (Gawenda et al., 1999). The resultant Pyrenean deformation was initially steady and continuous, causing minor compression landward of the Bay of Biscay (Jammes et al., 2009, 2010). The effect on deep-water sediment input was delayed, however, and only at ~53.5 Ma was a change seen from a calciclastic to siliciclastic turbidite system at Zumaia (Winkler and Gawenda, 1999). Variations in clay mineralogy at Zumaia are attributed to climatic variations and not to changing provenance or tectonic influence (Gawenda et al., 1999).

Initial stages of compression were felt at the northern Iberian border (Gräfe and Wiedmann, 1993) at ~55 Ma, progressing southward until ~46 Ma (Tugend et al., 2015). The Iberia Abyssal Plain site was distal from this tectonic centre during our study interval. The intensification of Iberia–Europe convergence did not occur until ~51 Ma (Roest and Sriverstava, 1991; Rosenbaum et al., 2002), also postdating our study intervals.

3.2. Palaeoceanographic setting

Turbidites were generally sourced from a mixed carbonate shelf in the east at Zumaia (Gawenda, 1999). Turbidite sands were derived from proto-equivalents of major river catchments that currently drain to the Iberian shelf (Marsaglia et al., 1996); hence a similar setting to the present day.

Circulation was predominantly driven by deep-water formation in the Southern Ocean during the Palaeocene and Eocene (Miller et al., 1987; Katz and Miller, 1991; Pak and Miller, 1992; Bralower et al., 1997; Norris et al., 2001), except around the IETM, where it reduced significantly (supplementary information; Kaminski et al., 1996; Norris et al., 2001, and references therein). Tethyan outflow temporarily dominated circulation, (Kaminski et al., 1996; Norris et al., 2001) which was probably similar to modern Mediterranean outflow (Corfield and Norris, 1996). The east Tethys was a probable source of high evaporation (Kaminski et al., 1996), which accelerated during intense warming at the IETM (Barron and Peterson, 1990). The short-term ocean circulation change intensified boundary currents in the west Atlantic, causing erosion at the Bermuda Rise between ~55.5 and 60 Ma (Norris et al., 2001). Lower Eocene hiatuses also exist in the North and South Atlantic at ~49 Ma (Tucholke, 1981; Aubry, 1995); however, these postdate our studied intervals.

Neither of our sites, nor any other Iberian and Bay of Biscay Deep Sea Drilling Program sites, show evidence for major erosion during the studied intervals. These sites show continuous sediment accumulation, absence of unconformities or hiatuses in deposition, and all biozones/subzones are identified (Canudo and Molina, 1992; Pak and Miller, 1992; Whitmarsh et al., 1998; Pardo et al., 1997; Ladner and Wise, 2001; McGonigal and Wise, 2001; Urquhart, 2001; Tremolada and Bralower, 2004).

Late Palaeocene–early Eocene Tethyan outflow flowed northward around the Iberian margin (Kaminski et al., 1996). The northern Bay of Biscay showed the influence of Tethyan waters, however, Zumaia registered only an Atlantic source (Kaminski et al., 1996), indicating it was distal to effects of bottom-currents.

Site 900, the shallowest continental slope site of Iberian ODP leg 149, sampled fine grained Palaeocene and Eocene contourites, but shows no evidence for erosion (Whitmarsh et al., 1998). The deeper water ODP sites locally show minor bottom-current influence but this is limited to slight winnowing of sandy turbidite tops (Whitmarsh et al., 1998); hemipelagic sediment accumulation rates are shown to be linear (Ladner and Wise, 2001; McGonigal and Wise, 2001).

4. Methods

4.1. Calculating recurrence intervals

Hemipelagic mud was deposited progressively in the time periods between turbidity currents. The thicknesses of hemipelagic mud intervals were converted to time periods by dividing by the rate of hemipelagic mud accumulation (Clare et al., 2014). Average hemipelagic mud accumulation rates were calculated using cumulative hemipelagic thickness between dated horizons. To do this, we must be able to identify hemipelagic mud intervals, and measure their thicknesses. The method assumes minimal fluctuations in hemipelagic mud accumulation rate between adjacent dated horizons. We therefore favour locations with better age control. It is also assumed there is little or no erosion of hemipelagic mud beneath turbidites. This assumption is based on the small depth of erosion seen in the available outcrop or core.

Hemipelagic mud intervals at Zumaia have thickness variations of $<$5 mm over distances of 50 m (extent of beach exposure) and trace fossils are not truncated (Bernaola et al., 2007). Turbidites logged from ODP site 1068 have flat bases and lack irregular bases indicative of erosion. The core is $\sim$10 cm in diameter. Erosional features with longer length scales would not be identified (Weaver and Thomson, 1993).

4.1.1. Identification of hemipelagic mud

Deposits logged visually by the authors have a vertical resolution of 5 mm. Hemipelagic mud can be clearly resolved from turbidite mud on the basis of colour and textural differences (Winkler and Gawenda, 1999; Bernaola et al., 2007; supplementary material). Turbidite thicknesses at Zumaia range from $<$5–170 mm over the studied interval, with a mean thickness of 16 mm. Turbidites in ODP 1068 range from 5–675 mm in thickness, with a mean thickness of 40 mm. The present day location of ODP Site 1068 is near the southern edge of the Iberia Abyssal Plain in 5044 m water depth, and its physiography is not interpreted to have changed much since the late Palaeocene (Whitmarsh et al., 1998). Both sites are interpreted as distal basin plain settings in accordance with the criteria of Mutti (1977). Bedding surfaces are even and parallel, turbidites are thin, typically base-missing Bouma sequences, grain size is limited to fine sand, with low to very low angle ripples often occurring in well-developed climbing patterns. Additionally, the considerable stratigraphic thickness of the sequences, trace fossils (Whitmarsh et al., 1998; Cummings and Hodgson, 2011) and benthic foraminiferal assemblages (Whitmarsh et al., 1998; Baceta et al., 2000) indicate a deep-water basin setting.

4.1.2. Age framework

Age control for the Zumaia section is based on biostratigraphy (Schmitz et al., 1997; Baceta et al., 2000; Alegret et al., 2009) and magnetostratigraphy (Baceta et al., 2000; Dinares-Turell et al., 2002; Storme et al., 2012). Dated horizons occur every 0.01 to 0.72 Myr within the Zumaia section and the interval containing the IETM is particularly well dated. This includes dates for subdivisions of the IETM, including onset, core (most intense), recovery and end phases of the Carbon Isotopic Excursion (CIE). This age control provides confidence in deriving hemipelagic accumulation rates and therefore recurrence intervals, particularly during and adjacent to the IETM. The rates of hemipelagic mud accumulation that we calculate show good correlation with those in previous studies (Winkler and Gawenda, 1999; Schmitz et al., 2001; supplementary material).

Age control for Iberia ODP Site 1068 is provided by biostratigraphy (Whitmarsh and Sawyer 1996; Whitmarsh et al., 1998; McGonigal and Wise, 2001; Ladner and Wise, 2001). Dated horizons occur every 0.7 to 1.0 Myr; hence dating is not as precise as at Zumaia; however, dates are available either side of the IETM to ensure confidence in its identification. Based on these dates and the vertical resolution, the minimum resolvable interval is 1.9 kyr at ODP Site 1068, compared to 0.5 kyr at Zumaia.

4.2. Carbon isotopic records

Negative δ^{13}C excursions are important because it has been proposed that they may relate to release of methane from gas hydrate in seafloor sediment, including via submarine landslides (Kennett et al., 2003; Maslin et al., 2004, 2010). Outcrop-specific δ^{13}C records based on whole-rock records are available for Zumaia (Gawenda et al., 1999; Schmitz et al., 2001). A direct comparison between turbidite frequency and the CIE can thus be made.

4.3. Comparison with sea level curve

Contrasting views of global sea level during the IETM exist (Sluijs et al., 2008). A sea level lowstand is inferred based on records from the North Atlantic (Neal and Hardenbol, 1998) and elsewhere (Schmitz and Pujalte, 2003), whereas Speijer and Morsi (2002) indicate a highstand in North Africa. Given these uncertainties, we do not compare turbidite recurrence intervals with sea level curves.

5. Results

5.1. Turbidite switch off during IETM

Turbidite recurrence intervals are broadly similar for most of the duration of two records studied here. The frequency distribution of turbidite recurrence intervals in the Zumaia section shows a good fit ($r^2 = 0.99$ based on least squares fit) to an exponential (Poisson) distribution (Fig. 2C). Some scatter is expected in the tail of exceedence plots due to limited data; however, five points lie well above the trend for a true Poisson distribution at Zumaia. Four of these relate to relatively long (25.1–35.2 kyr) recurrence intervals after the IETM, and one occurs during the IETM. The frequency distribution of turbidite recurrence intervals at the Iberian ODP Site 1068 location conform more closely to a log-normal distribution (Fig. 2B; $r^2 = 0.99$).

Running values of mean and standard deviation for recurrence intervals generally show variations of $<$10%, over a moving window of 50 beds (Fig. 3). However, a single anomalously

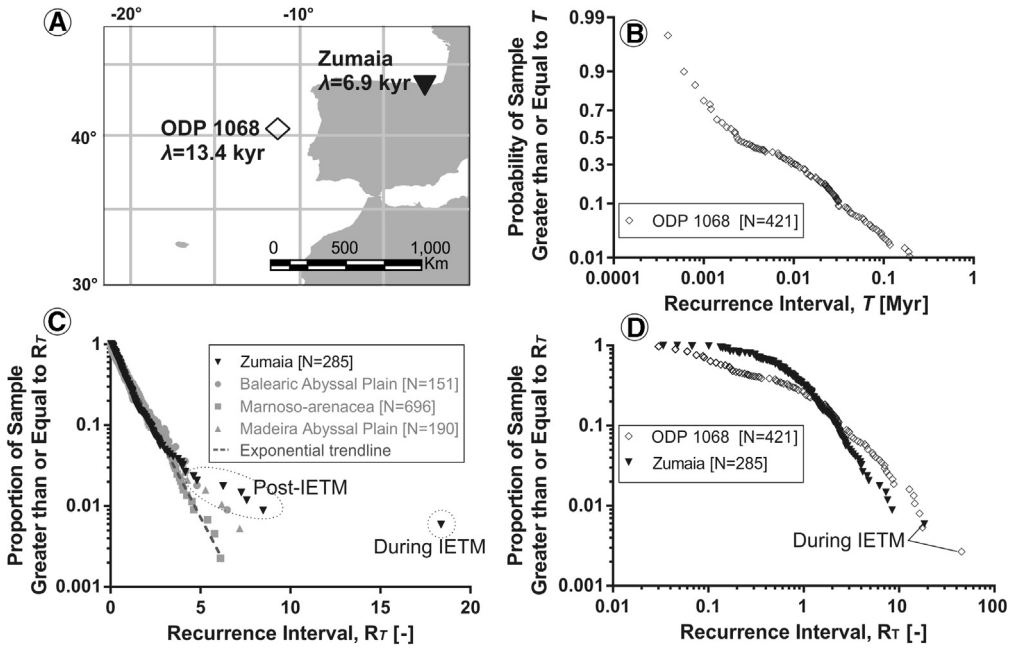

Fig. 2. (A) Location of study areas annotated with mean turbidite recurrence interval, λ. (B) Log-probability exceedence plot for ODP 1068 turbidite recurrence intervals showing a close approximation to a log-normal (straight line) trend. (C) Comparison of recurrence intervals on log-linear axes for Zumaia and sites in Clare et al. (2014) – data are normalised to mean recurrence interval, λ and generally show good agreement with an exponential (straight line) trend, except for data during IETM and some points following the IETM. (D) Comparison of Zumaia and ODP 1068 datasets on log–log axes showing outlying hiatuses found during the IETM.

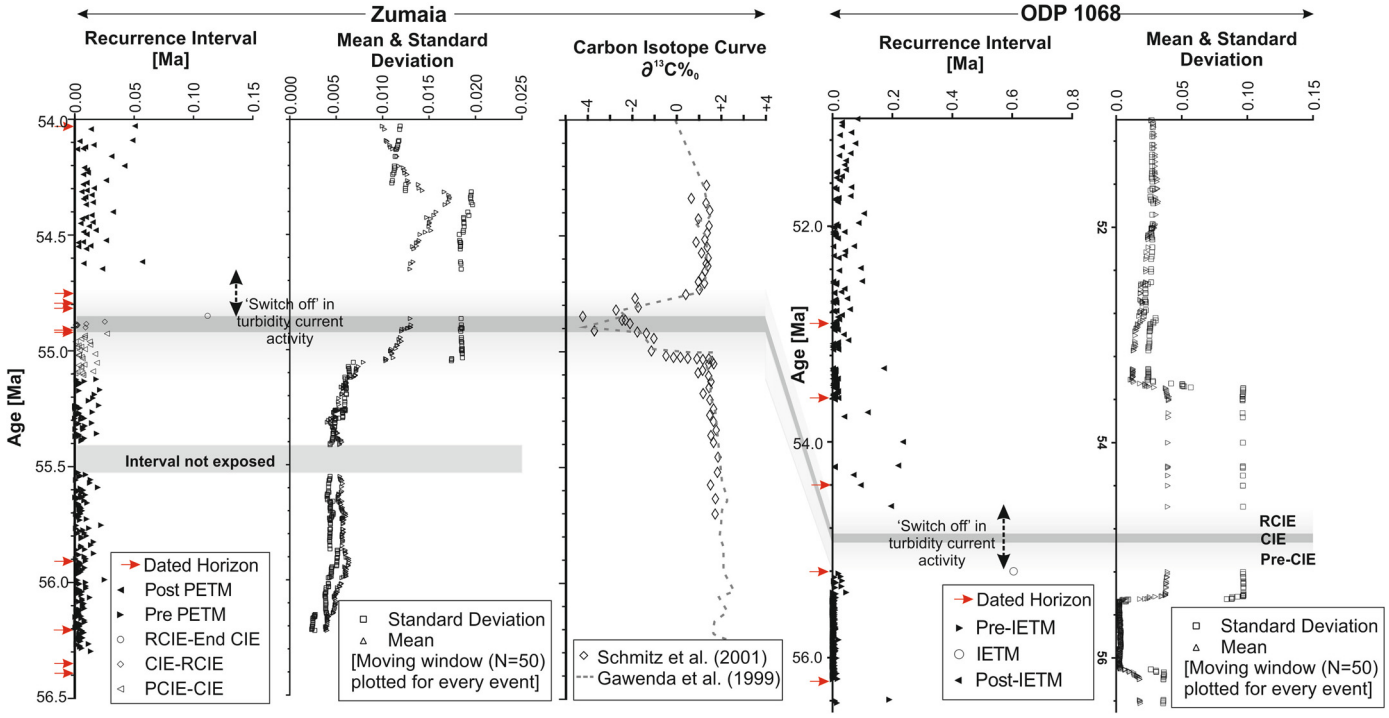

Fig. 3. Turbidite recurrence time series for Zumaia and ODP 1068 sites. Values of running mean and standard deviation for windows of 50 beds are highly skewed by anomalous hiatuses during with the IETM. Note change in age scale between sites. CIE = Carbon Isotopic Excursion; RCIE = Recovery Phase; PCIE = Pre-CIE.

long turbidite recurrence interval (Fig. 2D) occurs in both Zumaia (54.854–54.699 Ma) and ODP 1068 (55.2–54.595 Ma) datasets. The 155 kyr turbidite recurrence interval at Zumaia is far longer than the average recurrence interval of 7 kyr. Turbidites occur on average every 13 kyr in the ODP Site 1068 record, with an anomalous recurrence interval of 605 kyr. Interestingly, both anomalously long turbidite recurrence intervals coincide with the IETM.

5.1.1. Modelling of uncertainty in recurrence intervals

The precision of derived recurrence intervals can be affected by several variables. Erosion by successive turbidity currents, differential compaction and dewatering, and short-term decreases in background sedimentation rate may result in thinner hemipelagic beds. In contrast, short term increases in background sedimentation will yield thicker hemipelagic beds. Uncertainty in absolute dating of intervals may also arise from biostratigraphic and mag-

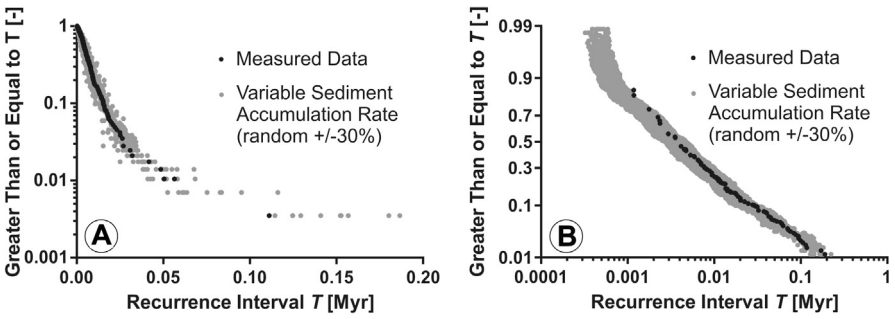

Fig. 4. Modelling of random variations (grey) in sediment accumulation rate between ±30% for Zumaia (A) and ODP site 1068 (B) compared with measured data (black) analysed in this study. Note that the general trends are well recreated providing confidence in our use of these data. This modelling accounts for short-term variations in hemipelagic sedimentation rates, as well as differential compaction, localised erosion, and uncertainties in age control of ±30%.

netostratigraphic data, which can lead to over- or under-estimation of recurrence intervals. To address these uncertainties we model variations in accumulation rate based on the measured data for each site to account for random variations of ±30% (Clare et al., 2014). We find that overall trends are well recreated, thus providing support for use of the data (Fig. 4). For ODP site 1068, there is some deviation from a straight line trend on a log-probability plot for intervals <0.001 Myr; however, these intervals are well below the resolution of the data and should not be considered valid (see also Fig. 4.)

5.1.2. Is the switch off genuine?

At both sites, the IETM interval is characterised by an approximately two to four-fold increase in background (hemipelagic) sediment accumulation rates, as noted by Winkler and Gawenda (1999) and Schmitz et al. (2001). Unlike the rest of the sequence which features hemipelagic marls and limestones, the non-turbidite deposits during the IETM comprise calcite-depleted clay – referred to as the 'siliciclastic unit' (Orue-Etxebarria et al., 2004; Schmitz et al., 1997; Schmitz et al., 2001). The paucity of calcite is attributed to dissolution in response to global ocean warming (Zachos et al., 2005). As both sites have age control points bounding the IETM, we can determine background hemiplegic accumulation rates for the 'siliciclastic unit'. At Zumaia, for example, hemipelagic accumulation rate increases from ~1 cm/kyr to 3 cm/kr at the start of the IETM (i.e. deposition was three times faster during the IETM). We correct for this using the age model and ensure that recurrence intervals are not overestimated based solely on bed thickness. Were we to just use hemipelagic mud thickness, the anomalous interval during the IETM would be >450 kyr; however our corrected value (which accounts for the increase in accumulation rates) is 155 kyr. We accept that there is likely to be some uncertainty in continuity of sediment accumulation rates between dated horizons; however, the anomalous interval is more than an order of magnitude greater than the mean trend. This is a significantly different result. We therefore suggest that the prolonged hiatuses in turbidity current activity at both sites are genuine.

5.2. Post-IETM reduction in turbidite frequency

We now consider variation in recurrence intervals, before, during and after the CIE at the IETM. We use a non-parametric approach as the distribution is non-Gaussian. We perform unpaired Mann–Whitney and Kolmogorov–Smirnov tests for recurrence intervals classified into different time periods. P values <0.05 allow us to conclude that the populations are significantly distinct and that random sampling could not account for this difference. Recurrence intervals are compared from periods relating to the entire dataset, before the IETM (56.311 to 55.127 Ma), pre-CIE to CIE (55.127 to 54.917 Ma), CIE to recovery phase (54.917 to 54.854

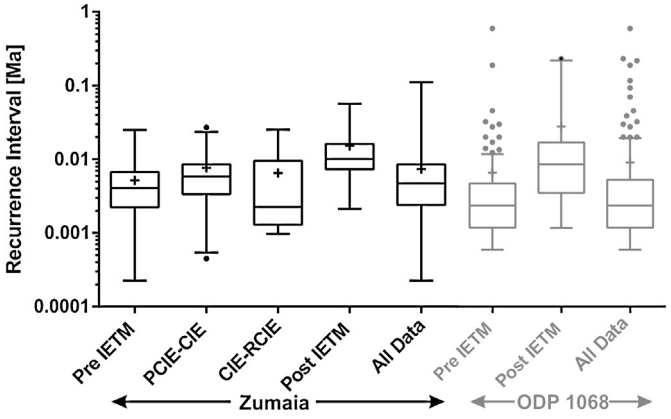

Fig. 5. Box and whisker plots of turbidite recurrence expressed for different time windows relative to the IETM. Boxes show 25% and 75% intervals, crosses indicate arithmetic mean values, whiskers show 5% and 95% intervals, and points represent values that fall outside 5% and 95% intervals. Post-IETM recurrence intervals are significantly longer than those Pre-IETM for both datasets.

Ma) and the interval post-IETM (54.749 to 54.482 Ma) for Zumaia. Interval dates are provided by the high resolution age and biostratigraphic framework of various authors (see supplementary material). Unlike ODP 1068, turbidites are identified during periods of the IETM at Zumaia; hence a higher resolution study is possible across the IETM interval. Only pre-IETM (56.390 to 55.127 Ma) and post-IETM (54.749 to 53.749 Ma) intervals are compared for the ODP 1068 site, where windows of one million years either side are selected for comparison (Fig. 5). The analysis shows that:

i) Mean and median recurrence intervals of the post-IETM window are significantly different ($p < 0.008$–0.001) to all the other time windows. For Zumaia, the mean recurrence interval prior to the IETM is 5 kyr, but increases after the IETM to 15.3 kyr. The mean recurrence is 7 kyr before the IETM at ODP Site 1068, and increases to 28 kyr for the 1 million year period after the IETM.
ii) At both sites, mean and median recurrence intervals before and during the $\delta^{13}C$ excursion are significantly different ($p < 0.01$) to recurrence after the IETM.

6. Discussion

In the following section, we first discuss the overall frequency distribution of turbidite recurrence at both sites and compare them with results from other basin plains. We then consider the anomalous switch off in turbidity current activity identified during the IETM, and the reduction in activity following the IETM. We compare our findings with published records from other IETM sites worldwide and explain the relevance for geohazard assessment. Fi-

nally, we explore wider implications for climate change in relation to submarine landslide activity.

6.1. Long term controls on turbidite recurrence

Turbidite recurrence intervals for the full record at Zumaia show a good agreement with an exponential (or Poisson) distribution for recurrence intervals <25 kyr. A common frequency distribution is observed in three deep-water basin plain settings worldwide (Fig. 2C; Clare et al., 2014). A Poisson distribution indicates random, time independent behaviour (Parzen, 1962); hence, it is unlikely that non-random processes such as sea level change exerted a dominant control on turbidite recurrence for most of the interval at Zumaia. However, recurrence intervals >25 kyr deviate significantly from the Poissonian background trend. These outliers either occur immediately after the IETM or during the IETM in the case of the longest recurrence interval. We suggest that effects of rapid climatic change during the IETM at Zumaia may have reduced the likelihood of turbidity current activity – both immediately before and during the IETM.

In contrast with Zumaia, an approximately log-normal distribution is identified for turbidite recurrence intervals at the ODP Site 1068. In the same manner that the *sum* of independent variables may yield a normal distribution, the *product* of several independent processes may create a log-normal distribution (van Rooij et al., 2013). This may result where a sequential series of processes controls turbidity current activity (Fig. 6). A simple example of multiplicative effects is shown as Eq. (1), where P is probability, LS denotes landslide and TC denotes turbidity current.

$$P_{(\text{TC at ODP 1068 site})} = P_{(\text{trigger generates LS})} \times P_{(\text{LS disintegrates to TC})} \times P_{(\text{TC runs out to site})} \quad (1)$$

A Poisson distribution is generated by additive independent effects, such as a random trigger, superimposition of multiple triggering processes, or several regional input sources. A hypothetical Poissonian additive probability for turbidite deposition at Zumaia, is shown in Eq. (2). A, B and C represent different source areas around the same basin margin.

$$P_{(\text{TC at Zumaia})} = P_{(\text{LS-triggered TC from A})} + P_{(\text{LS-triggered TC from B})} + P_{(\text{hyperpycnal-triggered TC from C})} \quad (2)$$

During the IETM, Zumaia was located ~30 km from the shelf break in a semi-enclosed basin setting (Schmitz et al., 2001) that may have featured sediment input from the north, south and west. ODP Site 1068 was located more distally (~200 km) from the shelf break, in an open setting, with a lower number of possible input sources. Therefore, the difference in frequency distribution form may be a function of basin morphology, nature and distance of input pathways, and the number of input sources. Regardless of frequency distribution form, however, both sites show an anomalous hiatus in turbidity current activity during the IETM (Fig. 1D) which is now the main focus of our discussion.

6.2. IETM-related control on landslide-turbidite recurrence intervals

The frequency of turbidity current activity is reduced significantly at the IETM. This includes a cessation of turbidity currents during the rapid warming phase, and a decrease in recurrence intensity immediately following the IETM (Fig. 5). We now explore the relevance to geohazard assessment and future climate changes studies.

6.2.1. Reduced landslide frequency during the IETM

We hypothesise that dramatic climatic effects during the IETM can explain the anomalous hiatuses and modifications in longer term recurrence trends. As the IETM features a major hiatus in activity, we can confidently state that no landslide-triggered turbidity currents (as well as those triggered by other processes) reached either site during that time. To account for uncertainty in whether turbidites are all landslide-triggered, we are circumspect about stating that changes in mean recurrence intervals are solely due to changes in landslide intensity. They may also relate to turbidity currents triggered by river flood discharge, canyon-flushing events or other processes. However, it is likely that a large proportion of the turbidites at these two sites was contributed by landslides. We therefore suggest that landslide activity decreased during the IETM, rather than increasing as predicted by previous studies (Kennett et al., 2003; Maslin et al., 2004, 2010).

6.2.2. Did flows route elsewhere during IETM?

The prolonged hiatuses observed at both Zumaia and ODP Site 1068 during the IETM are interpreted as a temporary "switch off" in turbidity current activity. Could it be that flows occurred, but simply did not reach these sites during this time, or else they were routed elsewhere? There is limited up-dip information that can be used to answer such questions unequivocally. A base of slope apron sequence is located 7 km to the SW of Zumaia at Ermua. Abundant turbidites and infrequent slump deposits complicate direct stratigraphic ties between Zumaia and Ermua. However, Schmitz et al. (2001) developed a high-resolution biostratigraphic and isotopic correlation across the IETM for these locations. Interpretation of stratigraphic logs (Schmitz et al., 2001) indicates a significant (greater than ten-fold) reduction in turbidity current activity at Ermua, coincident with the peak CIE at the IETM (Fig. 7). Turbidites emplaced during the IETM interval at Ermua are also considerably (<30%) thinner. Mean turbidite recurrence rate at Ermua is significantly less than at Zumaia, suggesting that not all flows make it to the basin plain, which is not unexpected. However, a decrease in turbidite recurrence at the start-IETM at Ermua provides support for a prolonged break in turbidity current activity.

6.2.3. Was there a tectonic influence?

The westward advance of the Pyrenean chain is not interpreted to have exerted a major influence on marine sedimentation until at least approximately 51 Ma which postdates the periods considered at our study areas (supplementary information). There is evidence for steady, independent movement of the Iberian Plate from ~55 Ma, however. Deformation was probably felt in the Pyrenean region initially but the effect at Zumaia was delayed until ~53.5 Ma (Winkler and Gawenda, 1999; Gawenda and Winkler, 2000) which corresponds to the later progradation of a deep sea fan (Cummings and Hodgson, 2011). Thus, this deformation also postdates our studied intervals. The initial stages of compression were focused far to the north of the Iberia Abyssal Plain and did not affect it, nor the eastward hinterland until much later (Gräfe and Wiedmann, 1993; Tugend et al., 2015). Major tectonic modification of sediment routing pathways is also not likely, as the provenance of turbidites did not change before or after the IETM at either of our sites (Marsaglia et al., 1996; Gawenda et al., 1999). Regardless of the interpretations above, if the sites were affected by major tectonic activity, we would expect an increase in turbidity current activity (e.g. Wagreich et al., 2011); instead we see a decrease in activity.

6.2.4. Did ocean circulation control turbidite frequency?

The influence of ocean warming at the IETM intensified Tethyan outflow (Norris et al., 2001 and references therein). A northward-

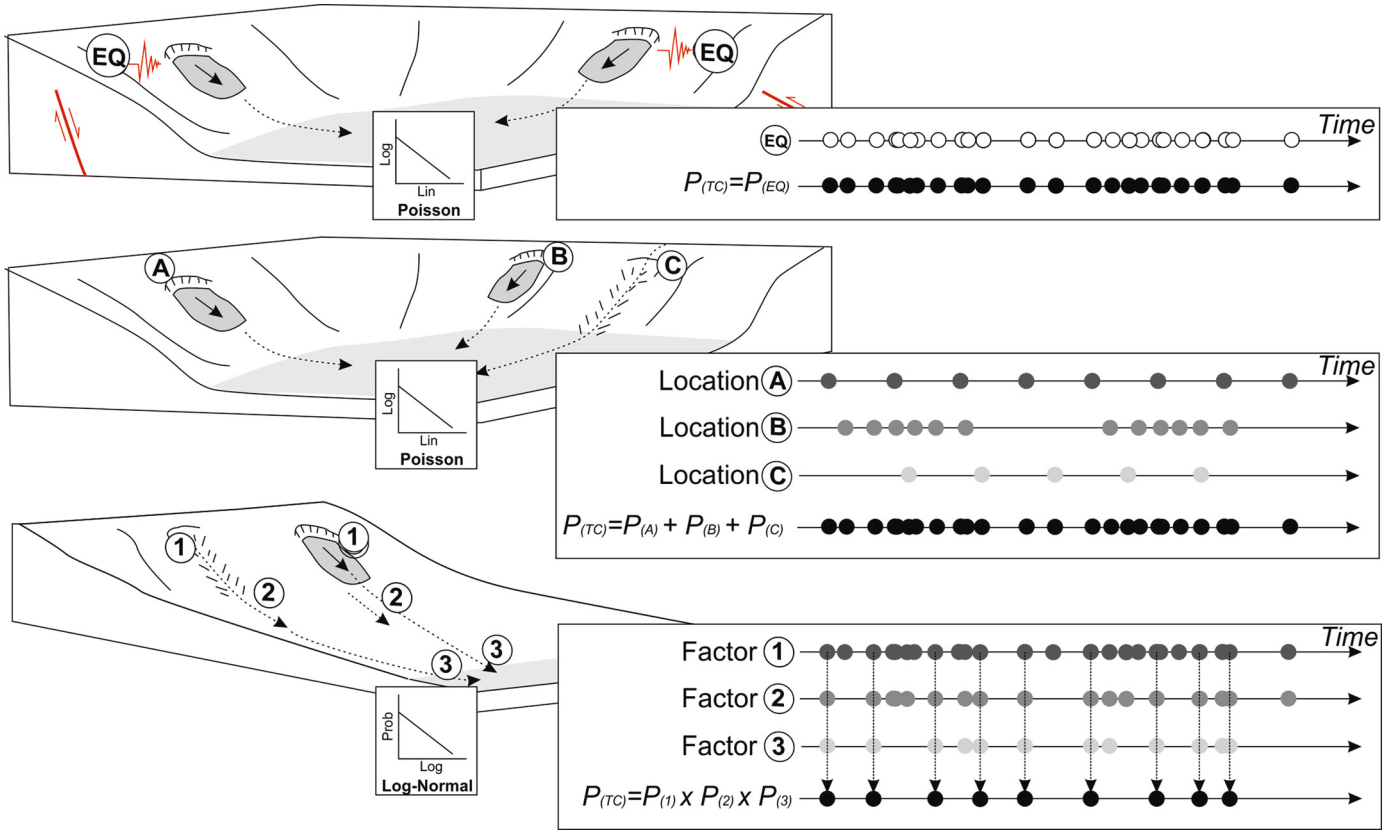

Fig. 6. Scenarios that generate different frequency distributions. Above: Poisson distribution assuming randomly distributed earthquake (EQ) trigger is responsible for each basin turbidite. Middle: Poisson distribution resulting from the sum of regional inputs to the basin which may include landslides on different margin flanks (A) and (B) and turbidity currents triggered by other processes (C) e.g. river floods. Below: Log-normal distribution in a more distal, open setting resulting from the product of probabilities. Basin turbidite frequency is the probabilistic product of landslides (1), disintegrating to become turbidity currents (2), which travel the distance to the basin plain (3).

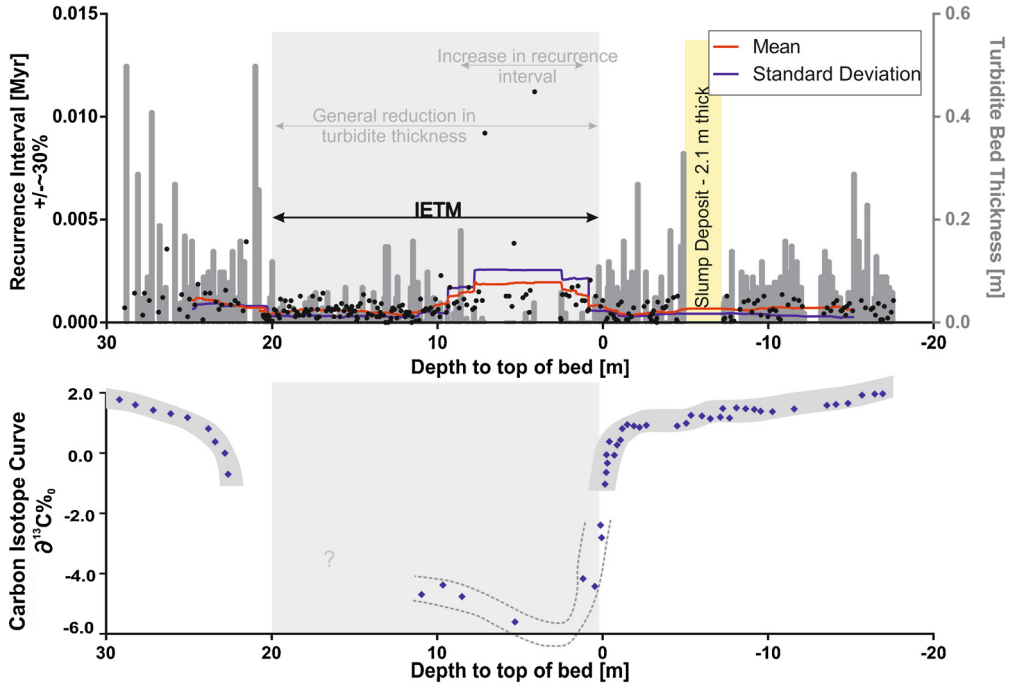

Fig. 7. Turbidite recurrence intervals for Ermua, NE Spain based on detailed lithostratigraphic logs from Schmitz et al. (2001). N = 211 turbidites. Age control is not well constrained; hence, the +/−30% uncertainty on recurrence intervals. This is used on the basis of assumptions in Clare et al. (2014). Erosion below base of beds cannot be discounted. At the onset IETM an anomalously long period of no turbidity current activity occurs. During the IETM, turbidites are generally thinner than the periods before and after.

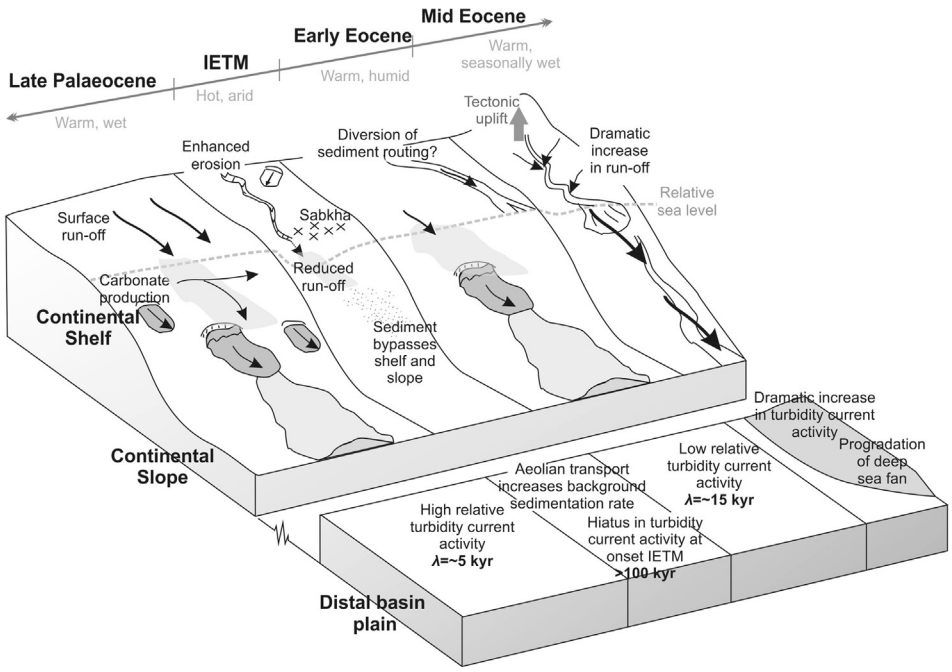

Fig. 8. Conceptual model explaining effects of climate change on deep-water turbidity current activity at Zumaia (distal basin plain).

flowing boundary current affected the Iberian margin (Whitmarsh and Sawyer, 1996). It is possible that a strengthened influence of contour currents may have temporarily starved the Iberia Abyssal Plain of turbidity flows due to interactions on the continental slope; however, other IETM sites (Section 6.3) including Zumaia (Kaminski et al., 1996) were not affected by bottom-currents and show a similar turbidite frequency response before, during and after the IETM (Kaminski et al., 1996). Therefore the localised effect of bottom-currents is not thought to have had a major effect on IETM turbidite frequency.

6.2.5. Why did turbidity current activity reduce post-IETM?

The background trend of recurrence appears to be largely insensitive to less acute, millennial oscillations in climate change. The pre-IETM interval was dominated at both sites by hemipelagic deposition interrupted by periodic turbidity currents – many of which were likely landslide-triggered. Warm and seasonally wet conditions are interpreted for the studied areas during this time (Gawenda and Winkler, 2000); but were dramatically altered to hot and arid at the onset-IETM, as indicated by terrestrial evaporite deposits (Schmitz and Pujalte, 2003). The IETM featured enhanced terrestrial erosion rates, but reduced hydrodynamic energy of freshwater outflow to the oceans in NE Spain (Schmitz et al., 2001). The elevation in deep marine background sedimentation rates (i.e. 'siliciclastic' unit) during the IETM is interpreted to be due to wind-blown transport (Schmitz et al., 2001), which also corroborates a hot, arid onshore setting. It is therefore possible that only minor fluvial/terrigenous contributions were made during the IETM to upper slope sedimentation, and did not provide conditioning for future landslides (i.e. no critical development of sediment thickness, slope steepening or excess pore pressures). This combination of factors may explain the reduction in both turbidity currents and landslides, as sediment was either locked up on land, bypassed the slope by aeolian transport, or was diverted by contour currents (Fig. 8). The modification of sediment routing pathways on land and on the continental shelf in response to dramatic climatic changes during the IETM may also explain the significantly different turbidite recurrence intervals following the IETM.

6.3. IETM turbidite frequency – global review

Most published IETM sections and boreholes were selected primarily for palaeoclimate studies, rather than turbidite frequency. As a consequence, there is a relative paucity of available data for a similar comparison. We summarise some existing studies (Fig. 9; Table 1) – many of which appear to corroborate our findings, although they are mostly qualitative in nature. Eight sites from Europe, Egypt and Newfoundland show a reduction in turbidity current activity during and/or after the IETM. In particular, the Anthering section in Austria (Egger et al., 2003) shows a decrease in turbidite sedimentation rate from 20 cm/kyr (pre-IETM) to 5 cm/kyr (post-IETM) which corresponds to a drop from 45 to 2 turbidites per metre. Unlike our sites, however, a dramatic increase in turbidite frequency is found immediately prior to the IETM. This may be climate-related, or could be due to an Alpine tectonic influence. Four sites from Europe, South Atlantic and Weddell Sea make no reference to turbidites, instead indicating continuous hemipelagic sequences during the IETM. A final example, in the Eastern Alps (Wagreich et al., 2011) shows a pronounced input of sand-rich turbidites during the IETM which is unlike all the other sites. This elevated sand input is interpreted to be a result of regional tectonic activity overprinting the effects of global climatic effects (Wagreich et al., 2011). This review indicates general agreement with our findings; however, there is a need for more detailed study. Future efforts should focus on similar deep-water sites to Zumaia and ODP Site 1068 to provide a greater number of observations for comparison.

6.4. Implications for geohazards

Our findings show that periods of future global ocean warming may not necessarily result in more frequent landslide and/or turbidity current activity on non-glacially influenced margins. This is relevant for future predictions of landslide-triggered tsunamis, as well as assessment of turbidity current impact on seafloor structures and cables. It may thus be appropriate to extrapolate geologically recent records of recurrence for future assessments. If we can relate recurrence intervals from the recent past, to field measurements in the present day, this strengthens the appropriateness

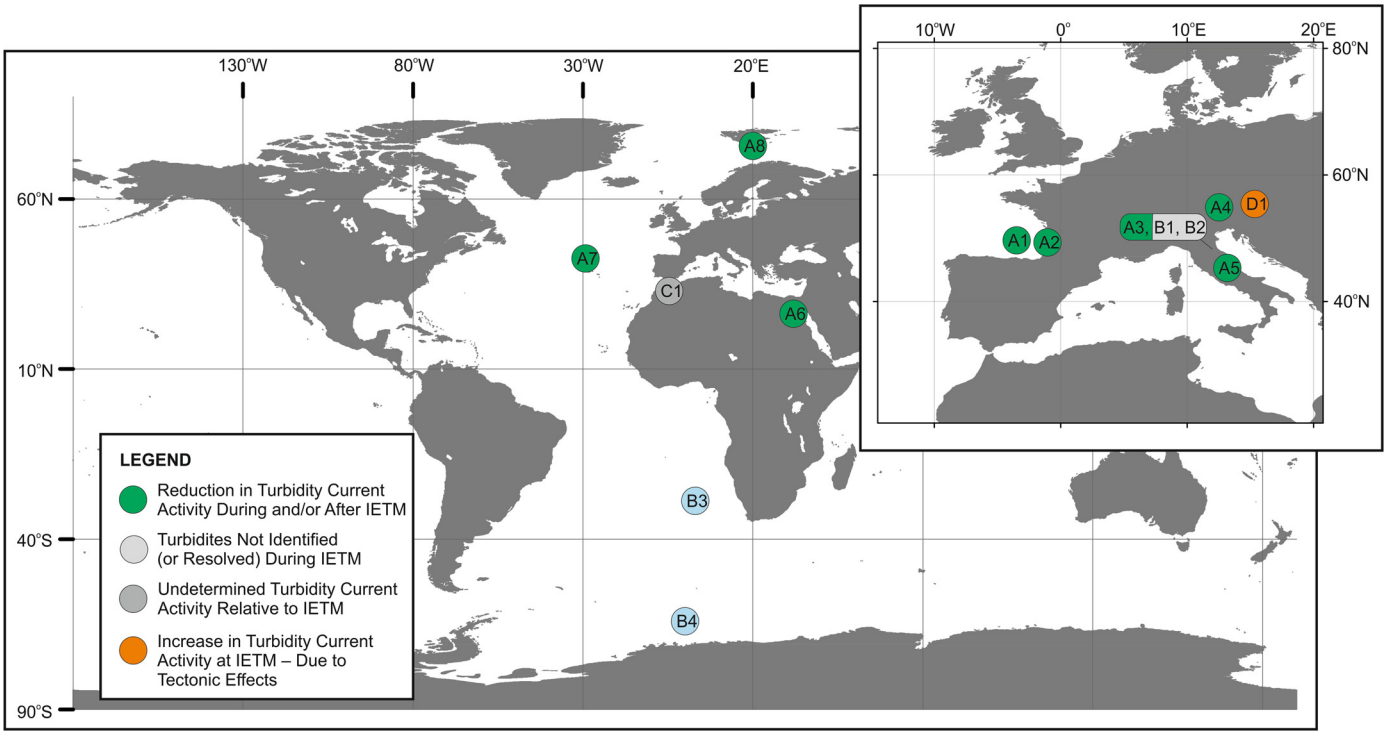

Fig. 9. Summary of other deep-water IETM sites with reference to turbidite recurrence. See Table 1 for details on locations and data sources.

of using this information for future assessment and mitigation. Turbidite records from other deep sea basins should be analysed during periods of rapid climate change to enhance confidence in future assessments. The Pacific and Indian Oceans are poorly sampled, so may be good candidates for future study.

6.5. Implications for future climate change

It has been proposed that landslide activity, and subsequent dissociation of gas hydrates, may have triggered the IETM (e.g. Kennett et al., 2003; Maslin et al., 2004; Katz et al., 2001). Our results, from local, detailed studies at two sites and a global review based on published literature, do not support this proposal. We do not identify a period of enhanced turbidity current activity prior to or at the start of the IETM, which would be expected if landslides were more common. If landslides were the primary source for methane release during the IETM, evidence is not seen at our sites. If release of buried methane is implicated in the onset of the IETM, an explanation may come from terrestrial climate effects. The transition from more humid to arid conditions at the start IETM (Schmitz et al., 2001) led to enhanced terrestrial erosion and could also have released methane from wetlands. Methane emissions from wetlands may exceed those from gas hydrates hosted in marine sediments, as suggested by isotopic analysis of methane within ice core records (Sowers, 2006).

Recent work actually argues that the likely amount of carbon mass input at the onset CIE (4000–7000 PgC) required a major alternative source of carbon in addition to any contribution from methane hydrates (Dunkley-Jones et al., 2010). A rapid CO_2-driven warming event is instead implicated for the cause of the negative $\delta^{13}C$ excursion (Sluijs et al., 2008). This warming event may have contributed to hydrate dissociation as part of a positive feedback loop. The extent of the gas hydrate stability zone during the IETM was likely less than the present day due to higher ambient temperatures (Dunkley-Jones et al., 2010). Therefore, the influence of marine hydrate dissociation on slope stability may have been relatively limited during the IETM.

It has been suggested that the periods such as the IETM present a possible proxy for understanding future anthropogenic climate change (e.g. Bowen et al., 2004), although they are not direct analogues (Haywood et al., 2011). Despite this, such intervals do provide valuable windows into the influence of warm climate states and elevated greenhouse gases on submarine sediment transport.

7. Conclusions

Several previous predictions suggested landslide and turbidity current activity should increase during periods of rapid global warming, due to dissociation of marine hydrates. Evidence from two deep-water sites indicates that the IETM corresponds to a reduction in turbidity current and landslide activity, and was followed by a period of reduced turbidity current and landslide activity. Our results have important implications for future landslide-triggered tsunami predictions, and assessment for subsea structures that maybe vulnerable to turbidity current impacts. Finally, we do not identify an increase in landslide activity prior to the IETM. We therefore suggest that globally widespread, landslide-triggered dissociation of hydrate may not be a likely cause for the negative $\delta^{13}C$ excursion during the IETM.

Acknowledgements

We thank Kyle Straub and two anonymous reviewers for their comments. This research used samples and data provided by the Ocean Drilling Program (ODP). ODP is sponsored by the U.S. National Science Foundation (NSF) and participating countries under management of Joint Oceanographic Institutions (JOI), Inc. This work is supported by the NERC Grant NE/K00008X/1.

Appendix A. Supplementary material

Supplementary material related to this article can be found online at http://dx.doi.org/10.1016/j.epsl.2015.03.022.

Table 1
Summary of other deep-water IETM sites with reference to turbidite recurrence. Location of sites is shown in Fig. 9.

Site ID	Site and Location	Palaeoenvironment (Water Depth)	Reference to Deposition Before, During and After IETM
Reduction in Turbidity Current Activity During and/or After IETM			
A1	Trabakua Pass, NE Spain (Schmitz et al., 2001)	Deep basin setting (~1000 m)	One major turbidite only identified during IETM, intervals before and after IETM feature many turbidites
A2	Ermua, NE Spain (Schmitz et al., 2001)	Base of slope apron	~160 turbidites within IETM (average ~1 cm thick). Anomalous hiatus coincident with carbon isotopic excursion. Either side of the IETM turbidites are thicker >~8 cm
A3	South Ardo, Southern Alps, NE Italy (Dallanave et al., 2012)	Deep marine	Some turbidites identified before IETM, but predominantly hemipelagite. No turbidites immediately post-IETM. A break in sequence means that the IETM itself is not preserved, however
A4	Anthering Section, Austria (Egger et al., 2003; Butt, 1981; Egger et al., 2009)	Continental rise (3000 m to 5000 m)	IETM features a threefold increase in bulk sedimentation rates. Turbidite sedimentation decreases from 20 cm/kyr (pre-IETM) to 5 cm/kyr (post-IETM), with a marked reduction in turbidity current activity during the IETM. Just before the IETM, a marked elevation in turbidity current activity is recorded. This record may also include tectonic effects however.
A5	Umbria–Marche, Central Italy, Contessa Highway Section (Galeotti et al., 2000)	Deep marine basin	Pelagic sediments only identified during IETM
A6	Galala Mountains, Egypt (Hontzsch et al., 2011; Speijer and Morsi, 2002; Speijer and Schmitz, 1998)	Carbonate ramp and basin	Transect of boreholes shows only marl and hemipelagite during IETM. Turbidites and debrites present before and after IETM interval.
A7	Newfoundland Basin, ODP Leg 210 (Tucholke and Sibuet, 2007)	Below CCD in basin plain	Multiple turbidites before IETM, but once Eocene commences, a switch to grainstone deposition occurred
A8	Svalbard, BH9/05 (Dypvik et al., 2011)	Open marine	Pre-IETM represented by sandy turbidites, but IETM and post-IETM appears to be shales (interpreted as hemipelagic mud)
Turbidites Not Identified (or Resolved)During IETM			
B1	Forada Section, Belluno Basin, NE Italy (Giusberti et al., 2007; Rohl et al., 2007; Luciani et al., 2007; Agnini et al., 2007)	Deep basin (~1000 ± 500 m)	Expanded sequence of clays and marls – no reference to any turbidites IETM documented to have a five-fold increase in bulk sedimentation rate and a decrease in grain size, rate which is attributed to increased weathering and run-off, but not turbidity current activity
B2	Possagno Section, Treviso, Belluno Basin, NE Italy (Agnini et al., 2006)	Deep water marine	Pink-reddish limestone to calcareous marlstone (pelagic to hemipelagic) succession is ascribed to the Scaglia Rossa. 14 m of finely bedded lower Eocene red calcareous marls identified during and post IETM. Turbidites only encountered in middle Eocene formation, not in late Palaeocene or early Eocene
B3	Walvis Ridge, South Atlantic – ODP Leg 208 ODP 1262, 1263, 1266 (Zachos et al., 2004; Chun et al., 2010)	Deep basin ODP 1262 (1500 m), ODP 1263 (2600 m) and ODP 1266 (3600 m)	Nannofossil ooze identified before and after IETM, and calcite-depleted clay during IETM with no indication of turbidites from core photos or shipboard logs
B4	Weddell Sea, ODP Site 690 (Rohl et al., 2007; Nielsen and Kelly, 2008)	Deep marine (1100–3600 m)	No reference made to turbidites before, during or after IETM
Undetermined Turbidity Current Activity Relative to IETM			
C1	Talaa Lakrah Flysch, Moroccan Rif Kaminski et al. (1996)	Lower bathyal or abyssal	Turbidites identified but no detail available on relative frequency in relation to IETM
Increase in Turbidity Current Activity at IETM – Due to Tectonic Effects			
D1	Gosau Group of Gams, Eastern Alps, Austria (Wagreich et al., 2011)	Open marine	Highly expanded IETM section with increased turbidite frequency at start Eocene. The pronounced input of sand fraction is interpreted by Wagreich et al. (2011) as a result of regional tectonic activity overprinting the effects of global environmental perturbations

References

Agnini, C., Fornaciari, E., Rio, D., Tateo, F., Backman, J., Giusberti, L., 2007. Responses of calcareous nannofossil assemblages, mineralogy and geochemistry to the environmental perturbations across the Paleocene/Eocene boundary in the Venetian Pre-Alps. Mar. Micropaleontol. 63 (1), 19–38.

Agnini, C., Muttoni, G., Kent, D.V., Rio, D., 2006. Eocene biostratigraphy and magnetic stratigraphy from Possagno, Italy: the calcareous nannofossil response to climate variability. Earth Planet. Sci. Lett. 241 (3), 815–830.

Alegret, L., Ortiz, S., Orue-Etxebarria, X., Bernaola, G., Baceta, J.I., Monechi, S., Pujalte, V., 2009. The Paleocene–Eocene thermal maximum: new data on microfossil turnover at the Zumaia section, Spain. Palaios 24 (5), 318–328.

Atwater, B.F., Griggs, G.B., 2012. Deep-sea turbidites as guides to Holocene earthquake history at the Cascadia Subduction Zone—alternative views for a seismic-hazard workshop. US Geol. Surv. Open-File Rep. 1043, 58.

Aubry, M.-P., 1995. From chronology to stratigraphy: interpreting the lower and middle Eocene stratigraphic record in the Atlantic Ocean. In: Berggren, W.A., Kent, D.V., Aubry, M.-P., Hardenbol, J. (Eds.), Geochronology, Time Scales and Global Stratigraphic Correlation. In: SEPM Special Publications, vol. 54, pp. 213–274.

Baceta, J.I., Pujalte, V., Dinares-Turrell, J., Payros, A., Orue-Etxebarria, X., Bernaola, G., 2000. The Palaeocene/Eocene boundary interval in the Zumaia Section (Gipuzkoa, Basque Basin): magnetostratigraphy and high-resolution lithostratigraphy. Rev. Soc. Geol. Esp. 13, 375–391.

Barron, E.J., Peterson, W.H., 1990. Mid-Cretaceous ocean circulation: results from model sensitivity studies. Paleoceanography 5 (3), 319–337.

Beattie, P.D., Dade, W.B., 1996. Is scaling in turbidite deposition consistent with forcing by earthquakes? J. Sediment. Res. 66 (5).

Bernaola, G., Baceta, J.I., Orue-Etxebarria, X., Alegret, L., Martín-Rubio, M., Arostegui, J., Dinarès-Turell, J., 2007. Evidence of an abrupt environmental disruption during the mid-Paleocene biotic event (Zumaia section, western Pyrenees). Geol. Soc. Am. Bull. 119 (7–8), 785–795.

Bock, J., Martinerie, P., Witrant, E., Chappellaz, J., 2012. Atmospheric impacts and ice core imprints of a methane pulse from clathrates. Earth Planet. Sci. Lett. 349, 98–108.

Bondevik, S., Løvholt, F., Harbitz, C., Mangerud, J., Dawson, A., Inge Svendsen, J., 2005. The Storegga Slide tsunami—comparing field observations with numerical simulations. Mar. Pet. Geol. 22 (1), 195–208.

Bowen, G.J., Beerling, D.J., Koch, P.L., Zachos, J.C., Quattlebaum, T., 2004. A humid climate state during the Palaeocene/Eocene thermal maximum. Nature 432 (7016), 495–499.

Bralower, T.J., Thomas, D., Zachos, J., et al., 1997. High resolution records of the late Palaeocene Thermal maximum and circum-Caribbean volcanism: is there a causal link? Geology 25, 963–966.

Brothers, D.S., Luttrell, K.M., Chaytor, J.D., 2013. Sea-level-induced seismicity and submarine landslide occurrence. Geology 41 (9), 979–982.

Bruschi, R., Bughi, S., Spinazzè, M., Torselletti, E., Vitali, L., 2006. Impact of debris flows and turbidily currents on seafloor structures. Nor. Geol. Tidsskr. 86 (3), 317.

Butt, A., 1981. Depositional environments of the Upper Cretaceous rocks in the northern part of the Eastern Alps. Spec. Pub. – Cushman Found. Foraminifer. Res. 20. 1981. pp. 1–81.

Canudo, J., Keller, G., Molina, E., Ortiz, N., 1995. Planktic foraminiferal turnover and $\delta^{13}C$ isotopes across the Paleocene–Eocene transition at Caravaca and Zumaya, Spain. Palaeogeogr. Palaeoclimatol. Palaeoecol. 114 (1), 75–100.

Canudo, J.I., Molina, E., 1992. Planktic foraminiferal faunal turnover and biochronostratigraphy of the Paleocene–Eocene boundary at Zumaya (Northern Spain). Rev. Soc. Geol. Esp. 5 (1–2), 145–157.

Carter, L., Burnett, D., Drew, S., Marle, G., Hagadorn, L., Bartlett-McNeil, D., Irvine, N., 2009. Submarine Cables and the Oceans—Connecting the World: United Nations Environment Programme. World Conservation Monitoring Center (UNEP-WCMC) Biodiversity Series, vol. 31. United Nations Environment Programme, World Conservation Monitoring Center, Cambridge, UK. http://www.unep-wcmc.org/resources/publications/UNEP_WCMC_bio_series/31.aspx. (accessed February 2014).

Carter, L., Milliman, J., Talling, P.J., Gavey, R., Wynn, R.B., 2012. Near-synchronous and delayed initiation of long run-out submarine sediment flows from a record breaking river flood, offshore Taiwan. Geophys. Res. Lett. 39, L12603. http://dx.doi.org/10.1029/2012GL051172.

Chun, C.O., Delaney, M.L., Zachos, J.C., 2010. Paleoredox changes across the Paleocene–Eocene thermal maximum, Walvis Ridge (ODP Sites 1262, 1263, and 1266): evidence from Mn and U enrichment factors. Paleoceanography 25 (4).

Clare, M.A., Talling, P.J., Challenor, P., Malgesini, G., Hunt, J., 2014. Distal turbidites reveal a common distribution for large (>0.1 km^3) submarine landslide recurrence. Geology. G35160-1.

Corfield, R.M., Norris, R.D., 1996. Deep water circulation in the Palaeocene ocean. In: Knox, R.W., Corfield, R.M., Dunay, R.E. (Eds.), Correlation of the Early Palaeogene in Northwest Europe. Geol. Soc. (Lond.) Spec. Publ. 101, 443–456.

Cummings, J.P., Hodgson, D.M., 2011. Assessing controls on the distribution of ichnotaxa in submarine fan environments, the Basque Basin, northern Spain. Sediment. Geol. 239 (3), 162–187.

Dallanave, E., Agnini, C., Muttoni, G., Rio, D., 2012. Paleocene magnetobiostratigraphy and climate-controlled rock magnetism from the Belluno Basin, Tethys Ocean, Italy. Palaeogeogr. Palaeoclimatol. Palaeoecol. 337, 130–142.

Dickens, G.R., O'Neil, J.R., Rea, D.K., Owen, R.M., 1995. Dissociation of oceanic methane hydrate as a cause of the carbon isotope excursion at the end of the Paleocene. Paleoceanography 10 (6), 965–971.

Dinarès-Turell, J., Baceta, J.I., Pujalte, V., Orue-Etxebarria, X., Bernaola, G., 2002. Magnetostratigraphic and cyclostratigraphic calibration of a prospective Palaeocene/Eocene stratotype at Zumaia (Basque Basin, northern Spain). Terra Nova 14 (5), 371–378.

Droxler, A.W., Schlager, W., 1985. Glacial versus interglacial sedimentation rates and turbidite frequency in the Bahamas. Geology 13 (11), 799–802.

Dunkley-Jones, T., Ridgwell, A., Lunt, D.J., Maslin, M.A., Schmidt, D.N.K., Valdes, P.J., 2010. A Palaeogene perspective on climate sensitivity and methane hydrate instability. Philos. Trans. R. Soc. A 368, 2395–2415.

Dypvik, H., Riber, L., Burca, F., Rüther, D., Jargvoll, D., Nagy, J., Jochmann, M., 2011. The Paleocene–Eocene thermal maximum (PETM) in Svalbard—clay mineral and geochemical signals. Palaeogeogr. Palaeoclimatol. Palaeoecol. 302 (3), 156–169.

Egger, H., Fenner, J., Heilmann-Clausen, C., Rogl, F., Sachsenhofer, R.F., Schmitz, B., 2003. Paleoproductivity of the northwestern Tethyan margin (Anthering section, Austria) across the Paleocene–Eocene transition. Spec. Pap., Geol. Soc. Am., 133–146.

Egger, H., Heilmann-Clausen, C., Schmitz, B., 2009. From shelf to abyss: record of the Paleocene/Eocene-boundary in the Eastern Alps (Austria). Geol. Acta 7 (1–2), 215–227.

Elmore, R.D., Pilkey, O.H., Cleary, W.J., Curran, H.A., 1979. Black shell turbidite, Hatteras abyssal plain, western Atlantic ocean. Geol. Soc. Am. Bull. 90 (12), 1165–1176.

Galeotti, S., Angori, E., Coccioni, R., Ferrari, G., Galbrun, B., Monechi, S., Turi, B., 2000. Integrated stratigraphy across the Paleocene/Eocene boundary in the Contessa Road section, Gubbio (central Italy). Bull. Soc. Géol. Fr. 171 (3), 355–365.

Gawenda, P., 1999. Climatic and tectonic controls on turbiditic and pelagic sedimentation in the deep sea: the Paleocene–Lower Eocene Zumaia Series (Northern Spain). Ph.D. thesis No. 13110. Swiss Federal Institute of Technology, Zurich, 213 pp.

Gawenda, P., Winkler, W., 2000. Sedimentary evolution of the early Paleogene deep-water Gulf of Biscay (proto-Atlantic): climatic and tectonic controls. Gff 122 (1), 54–55.

Gawenda, P., Winkler, W., Schmitz, B., Adatte, 1999. Climate and bioproductivity control on carbonate turbidite sedimentation (Palaeocene to Earliest Eocene, Gulf of Biscay, Zumaia, Spain). J. Sediment. Res. 69, 1253–1261.

Geist, E.L., Parsons, T., 2010. Estimating the empirical probability of submarine landslide occurrence. In: Mosher, D.C., Shipp, R.C., Moscardelli, L., Chaytor, J.D., Baxter, C.D.P., Lee, H.J., Urgeles, R. (Eds.), Submarine Mass Movements and Their Consequences. In: Advances in Natural and Technological Hazards Research, vol. 28, pp. 463–474.

Giusberti, L., Rio, D., Agnini, C., Backman, J., Fornaciari, E., Tateo, F., Oddone, M., 2007. Mode and tempo of the Paleocene–Eocene thermal maximum in an expanded section from the Venetian pre-Alps. Geol. Soc. Am. Bull. 119 (3–4), 391–412.

Goldfinger, C., Nelson, C.H., Johnson, J.E., 2003. Holocene earthquake records from the Cascadia subduction zone and northern San Andreas Fault based on precise dating of offshore turbidites. Annu. Rev. Earth Planet. Sci. 31 (1), 555–577.

Gräfe, K.U., Wiedmann, J., 1993. Sequence stratigraphy in the Upper Cretaceous of the Basco–Cantabrian basin (northern Spain). Geol. Rundsch. 82 (2), 327–361.

Grozic, J.L.H., 2010. Interplay between gas hydrates and submarine slope failure. In: Mosher, D.C., Shipp, R.C., Moscardelli, L., Chaytor, J.D., Baxter, C.D.P., Lee, H.J., Urgeles, R. (Eds.), Submarine Mass Movements and Their Consequences. In: Advances in Natural and Technological Hazards Research, vol. 28, pp. 463–474.

Haflidason, H., Lien, R., Sejrup, H.P., Forsberg, C.F., Bryn, P., 2005. The dating and morphometry of the Storegga Slide. Mar. Pet. Geol. 22 (1), 123–136.

Haywood, A.M., Ridgwell, A., Lunt, D.J., Hill, D.J., Pound, M.J., Dowsett, H.J., Williams, M., 2011. Are there pre-Quaternary geological analogues for a future greenhouse warming? Philos. Trans. R. Soc., Math. Phys. Eng. Sci. 369. 1938. pp. 933–956.

Höntzsch, S., Scheibner, C., Guasti, E., Kuss, J., Marzouk, A.M., Rasser, M.W., 2011. Increasing restriction of the Egyptian shelf during the Early Eocene?—new insights from a southern Tethyan carbonate platform. Palaeogeogr. Palaeoclimatol. Palaeoecol. 302 (3), 349–366.

Hornbach, M.J., Lavier, L.L., Ruppel, C.D., 2007. Triggering mechanism and tsunamogenic potential of the Cape Fear Slide complex, US Atlantic margin. Geochem. Geophys. Geosyst. 8 (12).

Hühnerbach, V., Masson, D.G., 2004. Landslides in the North Atlantic and its adjacent seas: an analysis of their morphology, setting and behaviour. Mar. Geol. 213, 343–362. http://dx.doi.org/10.1016/j.margeo.2004.10.013.

Hunt, J.E., Talling, P.J., Clare, M.A., Jarvis, I., Wynn, R.B., 2014. Long-term (17 Ma) turbidite record of the timing and frequency of large flank collapses of the Canary Islands. Geochem. Geophys. Geosyst. 15 (8), 3322–3345.

Hunt, J.E., Wynn, R.B., Talling, P.J., Masson, D.G., 2013. Frequency and timing of landslide-triggered turbidity currents within the Agadir Basin, offshore NW Africa: are there associations with climate change, sea level change and slope sedimentation rates? Mar. Geol. 346, 274–291.

Jammes, S., Lavier, L., Manatschal, G., 2010. Extreme crustal thinning in the Bay of Biscay and the Western Pyrenees: from observations to modeling. Geochem. Geophys. Geosyst. 11 (10).

Jammes, S., Manatschal, G., Lavier, L., Masini, E., 2009. Tectonosedimentary evolution related to extreme crustal thinning ahead of a propagating ocean: example of the western Pyrenees. Tectonics 28 (4).

Kaminski, M.A., Gradstein, F.M., Berggren, W.A., 1989. Paleogene benthic foraminifer biostratigraphy and paleoecology at Site 647, southern Labrador Sea. Proc. Ocean Drill. Program Sci. Results 105, 705–730.

Kaminski, M.A., Kuhnt, W., Radley, J.D., 1996. Palaeocene–Eocene deep water agglutinated foraminifera from the Numidian Flysch (Rif, Northern Morocco): their significance for the palaeoceanography of the Gibraltar gateway. J. Micropalaeontol. 15 (1), 1–19.

Katz, M.E., Cramer, B.S., Mountain, G.S., Katz, S., Miller, K.G., 2001. Uncorking the bottle: what triggered the Paleocene/Eocene thermal maximum methane release? Paleoceanography 16 (6), 549–562.

Katz, M.E., Miller, K.G., 1991. Early Palaeogene benthic foraminiferal assemblages and stable isotopes in the Southern Ocean. Proc. Ocean Drill. Program Sci. Results 114, 481–512.

Katz, M.E., Pak, D.K., Dickens, G.R., Miller, K.G., 1999. The source and fate of massive carbon input during the latest Paleocene thermal maximum. Science 286, 1531–1533.

Kennett, J.P., Cannariato, K.G., Hendy, I.L., Behl, R.J., 2003. Methane Hydrates in Quaternary Climate Change: The Clathrate Gun Hypothesis, vol. 54. American Geophysical Union, pp. 1–216.

Kennett, J.P., Stott, L.D., 1991. Abrupt deep-sea warming, palaeoceanographic changes and benthic extinctions at the end of the Palaeocene. Nature 353, 225–229.
Korup, O., Clague, J.J., Hermanns, R.L., Hewitt, K., Strom, A.L., Weidinger, J.T., 2007. Giant landslides, topography, and erosion. Earth Planet. Sci. Lett. 261 (3), 578–589.
Ladner, B.C., Wise, S.W. Jr., 2001. Calcareous nannofossil biostratigraphy of Upper Cretaceous to Paleocene sediments from Leg 173, Iberia Abyssal Plain, Sites 1067–1069. In: Beslier, M.-O., Whitmarsh, R.B., Wallace, P.J., Girardeau, J. (Eds.), Proc. ODP, Scientific Results, vol. 173, pp. 1–50.
Lee, H.J., 2009. Timing of occurrence of large submarine landslides on the Atlantic Ocean margin. Mar. Geol. 264, 53–64. Maslin 2009.
Luciani, V., Giusberti, L., Agnini, C., Backman, J., Fornaciari, E., Rio, D., 2007. The Paleocene–Eocene Thermal Maximum as recorded by Tethyan planktonic foraminifera in the Forada section (northern Italy). Mar. Micropaleontol. 64 (3), 189–214.
Marsaglia, K.M., Barragan, J.C.B., Padilla, I., Milliken, K.L., 1996. Evolution of the Iberian passive margin as reflected in sand provenance. Proc. Ocean Drill. Program Sci. Results, 269–280. National Science Foundation.
Maslin, M., Mikkelsen, N., Vilela, C., Haq, B., 1998. Sea-level- and gas-hydrate-controlled catastrophic sediment failures of the Amazon Fan. Geology 26 (12), 1107–1110.
Maslin, M., Owen, M., Betts, R., Day, S., Jones, T.D., Ridgwell, A., 2010. Gas hydrates: past and future geohazard? Philos. Trans. R. Soc., Math. Phys. Eng. Sci. 368 (1919), 2369–2393.
Maslin, M., Owen, M., Day, S., Long, D., 2004. Linking continental-slope failures and climate change: testing the clathrate gun hypothesis. Geology 32, 53–56.
Masson, D.G., Cartwright, J.A., Pinheiro, L.M., Whitmarsh, R.B., Beslier, M.O., Roeser, H., 1994. Compressional deformation at the ocean–continent transition in the NE Atlantic. J. Geol. Soc. 151 (4), 607–613.
Masson, D.G., Wynn, R.B., Talling, P.J., 2010. Large landslides on passive continental margins: processes, hypotheses and outstanding questions. In: Submarine Mass Movements and Their Consequences. Springer, Netherlands, pp. 153–165.
McGonigal, K.L., Wise, S.W. Jr., 2001. Eocene calcareous nannofossil biostratigraphy and sediment accumulation of turbidite sequences on the Iberia Abyssal Plain, ODP Sites 1067–1069. In: Beslier, M.-O., Whitmarsh, R.B., Wallace, P.J., Girardeau, J. (Eds.), Proc. ODP, Scientific Results, vol. 173, pp. 1–35.
McInerney, F.A., Wing, S.L., 2011. The Paleocene–Eocene thermal maximum: a perturbation of carbon cycle, climate, and biosphere with implications for the future. Annu. Rev. Earth Planet. Sci. 39, 489–516.
Miller, K.G., Janecek, T.R., Katz, M.E., Keil, D.J., 1987. Abyssal circulation and benthic foraminiferal changes near the Paleocene/Eocene boundary. Paleoceanography 2 (6), 741–761.
Mutti, E., 1977. Distinctive thin-bedded turbidite facies and related depositional environments in the Eocene Hecho Group (South-central Pyrenees, Spain). Sedimentology 24 (1), 107–131.
Neal, J.E., Hardenbol, J., 1998. Introduction to the Paleogene. In: de Graciansky, P.-C., et al. (Eds.), Mesozoic and Cenozoic Sequence Stratigraphy of European Basins. In: SEPM (Society for Sedimentary Geology) Special Publication, vol. 60, pp. 87–90.
Nielsen, T.M., Kelly, D.C., 2008. Planktic foraminiferal assemblage variations associated with the Paleocene–Eocene thermal maximum: high latitude ODP Site 689 (Maud Rise, Weddell Sea). Mar. Micropaleontol.
Nisbet, E.G., Piper, D.J., 1998. Giant submarine landslides. Nature 392 (6674), 329–330.
Normark, W.R., Piper, D.J.W., 1991. Initiation processes and flow evolution of turbidity currents: implications for the depositional record. In: Osborne, R.H. (Ed.), From Shoreline to Abyss: Contributions in Marine Geology in Honor of Francis Parker Shepard. Spec. Publ., Soc. Econ. Paleontol. Mineral. 46, 230.
Norris, R.D., Klaus, A., Kroon, D., 2001. Mid-Eocene deep water, the Late Palaeocene Thermal maximum and continental slope mass wasting during the Cretaceous-Palaeogene Impact. Geol. Soc. (Lond.) Spec. Publ. 183, 23–48.
Orue-Etxebarria, X., Bernaola, G., Baceta, J.I., Angori, E., Caballero, F., Monechi, S., Payros, A., 2004. New constraints on the evolution of planktic foraminifers and calcareous nannofossils across the Palaeocene–Eocene boundary interval: the Zumaia section revisited. Neues Jahrb. Geol. Paläontol. Abh. 234 (1–3), 223–260.
Owen, M., Day, S., Maslin, M., 2007. Late Pleistocene submarine mass movements: occurrence and causes. Quat. Sci. Rev. 26, 958–978.
Pak, D.K., Miller, K.G., 1992. Paleocene to Eocene benthic foraminiferal isotopes and assemblages: implications for deepwater circulation. Paleoceanography 7 (4), 405–422.
Pardo, A., Keller, G., Molina, E., Canudo, J., 1997. Planktic foraminiferal turnover across the Paleocene–Eocene transition at DSDP Site 401, Bay of Biscay, North Atlantic. Mar. Micropaleontol. 29 (2), 129–158.
Parzen, E., 1962. On estimation of a probability density function and mode. Ann. Math. Stat. 33 (3), 1065–1076.
Pilkey, O.H., 1988. Basin plains; giant sedimentation events. Spec. Pap., Geol. Soc. Am. 229, 93–100.
Pinheiro, L.M., Wilson, R.C.L., Pena dos Reis, R., Whitmarsh, R.B., Ribeiro, A., 1996. The western Iberia Margin: a geophysical and geological overview. In: Whitmarsh, R.B., Sawyer, D.S., Klaus, A., Masson, D.G. (Eds.), Proc. ODP, Sci. Results 149, 3–23. College Station TX (Ocean Drilling Program).
Piper, D.J.W., Cochonat, P., Morrison, M.L., 1999. The sequence of events around the epicenter of the 1929 Grand Banks earthquake: initiation of the debris flows and turbidity current inferred from side scan sonar. Sedimentology 46, 79–97. http://dx.doi.org/10.1046/j.1365-3091.1999.00204.x.
Piper, D.J., Normark, W.R., 2009. Processes that initiate turbidity currents and their influence on turbidites: a marine geology perspective. J. Sediment. Res. 79 (6), 347–362.
Piper, D.J., Savoye, B., 1993. Processes of late Quaternary turbidity current flow and deposition on the Var deep-sea fan, north-west Mediterranean Sea. Sedimentology 40 (3), 557–582.
Roest, W.R., Srivastava, S.P., 1991. Kinematics of the plate boundaries between Eurasia, Iberia, and Africa in the North Atlantic from the Late Cretaceous to the present. Geology 19 (6), 613–616.
Röhl, U., Westerhold, T., Bralower, T.J., Zachos, J.C., 2007. On the duration of the Paleocene–Eocene thermal maximum (PETM). Geochem. Geophys. Geosyst. 8 (12).
Romans, B.W., Normark, W.R., McGann, M.M., Covault, J.A., Graham, S.A., 2009. Coarse-grained sediment delivery and distribution in the Holocene Santa Monica Basin, California: implications for evaluating source-to-sink flux at millennial time scales. Geol. Soc. Am. Bull. 121 (9–10), 1394–1408.
Rosenbaum, G., Lister, G.S., Duboz, C., 2002. Relative motions of Africa, Iberia and Europe during Alpine orogeny. Tectonophysics 359 (1), 117–129.
Schmitz, B., Asaro, F., Molina, E., Monechi, S., von Salis, K., Speijer, R.P., 1997. High-resolution iridium, δ13C, δ18O, foraminifera and nannofossil profiles across the latest Paleocene benthic extinction event at Zumaya, Spain. Palaeogeogr. Palaeoclimatol. Palaeoecol. 133 (1), 49–68.
Schmitz, B., Pujalte, V., Nunez-Betelu, K., 2001. Climate and sea-level perturbations during the incipient Eocene thermal maximum: evidence from siliciclastic units in the Basque Basin (Ermua, Zumaia and Trabakua Pass), northern Spain. Palaeogeogr. Palaeoclimatol. Palaeoecol. 165 (3), 299–320.
Schmitz, B., Pujalte, V., 2003. Sea-level, humidity, and land-erosion records across the initial Eocene thermal maximum from a continental-marine transect in northern Spain. Geology 31 (8), 689–692.
Sluijs, A., Brinkhuis, H., Crouch, E.M., John, C.M., Handley, L., Munsterman, D., Dickens, G.R., 2008. Eustatic variations during the Paleocene–Eocene greenhouse world. Paleoceanography 23 (4).
Sowers, T., 2006. Late Quaternary atmospheric CH4 isotope record suggests marine clathrates are stable. Science 311 (5762), 838–840.
Speijer, R.P., Morsi, A.M.M., 2002. Ostracode turnover and sea-level changes associated with the Paleocene–Eocene thermal maximum. Geology 30 (1), 23–26.
Speijer, R.P., Schmitz, B., 1998. A benthic foraminiferal record of Paleocene sea level and trophic/redox conditions at Gebel Aweina, Egypt. Palaeogeogr. Palaeoclimatol. Palaeoecol. 137 (1), 79–101.
Storme, J.Y., Devleeschouwer, X., Schnyder, J., Cambier, G., Baceta, J.I., Pujalte, V., Yans, J., 2012. The Palaeocene/Eocene boundary section at Zumaia (Basque–Cantabric Basin) revisited: new insights from high-resolution magnetic susceptibility and carbon isotope chemostratigraphy on organic matter (δ^{13}Corg). Terra Nova 24 (4), 310–317.
Talling, P.J., Amy, L.A., Wynn, R.B., 2007. New insights into the evolution of large volume turbidity currents; comparison of turbidite shape and previous modelling results. Sedimentology 54, 737–769.
Talling, P., Clare, M., Urlaub, M., Pope, E., Hunt, J., Watt, S., 2014. Large submarine landslides on continental slopes: geohazards, methane release and climate change. Oceanography 27 (2), 32–45.
Talling, P.J., Masson, D.G., Sumner, E.J., Malgesini, G., 2012. Subaqueous sediment density flows: depositional processes and deposit types. Sedimentology 59 (7), 1937–2003.
Talling, P.J., Paull, C.K., Piper, D.J., 2013. How are subaqueous sediment density flows triggered, what is their internal structure and how does it evolve? Direct observations from monitoring of active flows. Earth-Sci. Rev. 125, 244–287.
Talling, P.J., 2014. On the triggers, resulting flow types and frequencies of subaqueous sediment density flows in different settings. Mar. Geol. http://dx.doi.org/10.1016/j.margeo.2014.02.006.
Tappin, D.R., Watts, P., McMurtry, G.M., Lafoy, Y., Matsumoto, T., 2001. The Sissano, Papua New Guinea tsunami of July 1998—offshore evidence on the source mechanism. Mar. Geol. 175 (1), 1–23.
Tremolada, F., Bralower, T.J., 2004. Nannofossil assemblage fluctuations during the Paleocene–Eocene thermal maximum at Sites 213 (Indian Ocean) and 401 (North Atlantic Ocean): palaeoceanographic implications. Mar. Micropaleontol. 52 (1), 107–116.
Tucholke, B.E., 1981. Geologic significance of seismic reflectors in the deep western North Atlantic basin.
Tucholke, B.E., Sibuet, J.C., 2007. Leg 210 synthesis: tectonic, magmatic, and sedimentary evolution of the Newfoundland-Iberia rift. Proc. Ocean Drill. Program Sci. Results 210, 1–56.
Tugend, J., Manatschal, G., Kusznir, N.J., 2015. Spatial and temporal evolution of hyperextended rift systems: implication for the nature, kinematics, and timing of the Iberian–European plate boundary. Geology 43 (1), 15–18.

Urlaub, M., Talling, P.J., Masson, D.G., 2013. Timing and frequency of large submarine landslides: implications for understanding triggers and future geohazard. Quat. Sci. Rev. 72, 63–82.

Urlaub, M., Talling, P., Clare, M., 2014. Sea-level-induced seismicity and submarine landslide occurrence: comment. Geology 42 (6).

Urquhart, E., 2001. Campanian to Miocene planktonic foraminifers from the Iberia abyssal plain. Proc. Ocean Drill. Program Sci. Results 173.

van Rooij, M.M., Nash, B.A., Rajaraman, S., Holden, J.G., 2013. A fractal approach to dynamic inference and distribution analysis. Front. Physiol. 4.

Vergés, J., Millán, H., Roca, E., Muñoz, J.A., Marzo, M., Cirés, J., Cloetingh, S., 1995. Eastern Pyrenees and related foreland basins: pre-, syn- and post-collisional crustal-scale cross-sections. Mar. Pet. Geol. 12 (8), 903–915.

Wagreich, M., Egger, H., Gebhardt, H., Mohammed, O., Spötl, C., Koukal, V., Hobiger, G., 2011. A new expanded record of the Paleocene–Eocene transition in the Gosau Group of Gams (Eastern Alps Austria). Ann. Naturhistor. Museums Wien. Ser. A, 35–65.

Weaver, P.P.E., Rothwell, R.G., Ebbing, J., Gunn, D., Hunter, P.M., 1992. Correlation, frequency of emplacement and source directions of megaturbidites on the Madeira Abyssal Plain. Mar. Geol. 109 (1), 1–20.

Weaver, P.P.E., Searle, R.C., Kuijpers, A., 1986. Turbidite deposition and the origin of the Madeira Abyssal Plain. Geol. Soc. (Lond.) Spec. Publ. 21 (1), 131–143.

Weaver, P.P.E., Thomson, J., 1993. Calculating erosion by deep-sea turbidity currents during initiation and flow. Nature 364, 136–138. http://dx.doi.org/10.1038/364136a0.

Whitmarsh, R.B., Beslier, M.O., Wallace, P.J., 1998. Return to Iberia. Proc. Ocean Drill. Program Init. Reports 173.

Whitmarsh, R.B., Sawyer, D.S., 1996. The ocean/continent transition beneath the Iberia Abyssal Plain and continental-rifting to seafloor-spreading processes. Proc. Ocean Drill. Program Sci. Results, 713–736. National Science Foundation.

Winkler, W., Gawenda, P., 1999. Distinguishing climatic and tectonic forcing of turbidite sedimentation, and the bearing on turbidite bed scaling: Palaeocene–Eocene of northern Spain. J. Geol. Soc. 156 (4), 791–800.

Zachos, J.C., Kroon, D., Blum, P., et al., 2004. Proc. ODP, Init. Repts., 208. College Station, TX (Ocean Drilling Program) http://dx.doi.org/10.2973/odp.proc.ir.208.2004.

Zachos, J.C., Röhl, U., Schellenberg, S.A., Sluijs, A., Hodell, D.A., Kelly, D.C., Thomas, E., Nicolo, M., Raffi, I., Lourens, L.J., McCarren, H., Kroon, D., 2005. Rapid acidification of the ocean during the Paleocene–Eocene thermal maximum. Science 308 (5728), 1611–1615.